Charge Redistribution and Extraction in Photocatalytically Synthesized Au–ZnO Nanohybrids

ARTICLE *in* THE JOURNAL OF PHYSICAL CHEMISTRY C · AUGUST 2015

Impact Factor: 4.77 · DOI: 10.1021/acs.jpcc.5b06520

THE JOURNAL OF PHYSICAL CHEMISTRY C

Article

pubs.acs.org/JPCC

Charge Redistribution and Extraction in Photocatalytically Synthesized Au−ZnO Nanohybrids

Alina Chanaewa,*[,†,‡] Julius Schmitt,[‡] Michaela Meyns,[⊥] Mirjam Volkmann,[∥] Christian Klinke,[∥] and Elizabeth von Hauff[§]

[†]Fraunhofer ISE, 79110 Freiburg, Germany

[‡]Institute of Physics, University of Freiburg, 79104 Freiburg, Germany

[⊥]Catalonia Institute for Energy Research, 08930 Barcelona, Spain

[∥]Institute of Physical Chemistry, University of Hamburg, 20146 Hamburg, Germany

[§]Physics of Energy, VU University Amsterdam, 1081 HV Amsterdam, Netherlands

Supporting Information

ABSTRACT: ZnO is a promising catalyst for hydrogen and oxygen production due to the position of the conduction and valence bands. Nevertheless, there are some limitations to the efficiency due to its n-type character. Once in contact with the electrolyte, an extraction barrier for electrons is formed. The purpose of this work was to create an extraction site for electrons by synthesizing small pyramidally shaped ZnO nanocrystals (∼10 nm), which consist of a predefined site for the growth of a gold particle at the tip. Photoelectrochemical deposition of gold on ZnO was performed to yield the hybrid structure. Photoluminescence (PL) studies of the relative change of intensities of band gap versus defect state relaxation showed electron transfer from the conduction band of ZnO to Au. Using cyclic voltammetry, Au-mediated charge extraction from Au−ZnO hybrids was demonstrated, which circumvents the electron extraction barrier in ZnO. Thus, this work demonstrates the nanoscale design of hybrid structures for photocatalytic applications.

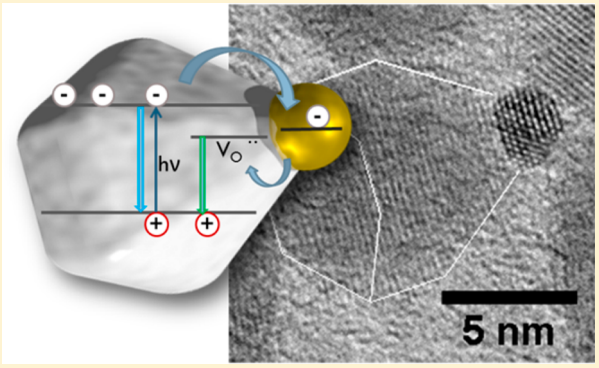

INTRODUCTION

One of the major challenges in the area of energy generation is the efficient use of solar energy for photoelectrochemical water splitting.[1−3] Since the water splitting reaction is thermodynamically highly unfavored, the use of an efficient catalyst for both hydrogen and oxygen evolution is crucial. Unfortunately, the choice of catalyst is governed by several compromises. The ideal semiconductor catalyst should be able to generate both hydrogen and oxygen. That means that the conduction band edge should be energetically matched to the hydrogen redox potential of 0 V vs NHE and the valence band edge should be matched with the oxygen redox potential of 1.23 V vs NHE. The consequence is that the choice of semiconductors is theoretically restricted to a band gap of 1.23 eV or even larger due to overpotentials in the electrochemical system.[4] Generally, metal oxides such as ZrO_2, $KTaO_3$, $SrTiO_3$, TiO_2, and ZnO meet the above-mentioned criteria. The major drawback for applications that are dependent on solar energy is that the optical absorption of these materials lies in the UV range of the solar spectrum due to the wide band gaps of more than 3 eV so that only a small part of the incident energy can be converted. Nevertheless, ZnO has received strong attention as promising catalyst due to its innocuousness, abundance, facile synthesis allowing for versatile shapes and sizes, and its easy surface modification.[5−7]

Heterogeneous catalysis is governed by the catalyst surface, i.e. size, area, and morphology as well as the ability to transfer charges. A large surface is beneficial and is achieved by reducing the semiconductor size to a few nanometers. Since ZnO is an n-type semiconductor, it forms a Schottky barrier with surrounding electrolyte.[8] Consequently, it prevents electron extraction, thus suppressing hydrogen production. The behavior is well-known for bulk ZnO but was also shown for some small particles[9] and therefore has to be considered for catalyst design. This issue can be circumvented by defining additional extraction sites for electrons and changing the electronic structure of the catalyst. The photochemical activity of TiO_2 nanoparticles (NPs) was shown to increase upon attaching gold particles to the metal oxide surface.[10] UV illumination leads to electron transfer from the metal oxide to the noble metal particle inducing charge redistribution between TiO_2 and Au. Electron accumulation on the gold particle means

Received: July 7, 2015
Revised: August 26, 2015
Published: August 31, 2015

DOI: 10.1021/acs.jpcc.5b06520
J. Phys. Chem. C 2015, 119, 21704−21710

that the Fermi level increases to more negative potentials, approaching the conduction band TiO_2. Successful fullerene reduction demonstrated that gold facilitates charge separation and charge transfer to the electrolyte.[11] Charge redistribution in the Au−ZnO nanosystem was spectroscopically shown and discussed by Wood et al.,[12] leading to similar conclusions found for Au−TiO_2.

Our goal is to create a well-defined Au−ZnO system for photocatalytic water splitting, where an Au particle is attached on a predefined site for efficient electron extraction. This can be realized by controlling the morphology of ZnO NPs via precise adjustment of reaction condition and surfactants. This is considerably more difficult to realize for small particles compared to larger ones[13−16] where thermodynamic control occurs on a longer time scale. Various synthetic routes are described in the literature which yield pyramidal particles of the size of few tens of nanometers[17−20] and significantly larger,[21−23] which usually do not require any additional surfactant and the growth is purely thermodynamically driven. Smaller pyramidal shaped particles demonstrated a significantly broader size distribution and an erratic shape compared to larger particles in the case of growth driven by pure thermodynamic control.[23]

First, we demonstrate the controlled synthesis of 10 nm sized pyramidally shaped ZnO NPs under ambient conditions. Au is subsequently photocatalytically deposited on the pyramid tip under UV illumination, forming 4 nm sized spherical particles. The advantage of photoreduction of gold is the high selectivity of the deposition site, which was found to be at the tip of the pyramidal structures. Use of an additional reducing agent was shown to yield gold nanoparticles on alternating sites lacking selectivity.[23] Density functional theory (DFT) calculations were utilized to investigate the role of ligands in selective attachment of gold to the tip of ZnO pyramids.

To determine the catalytic suitability of the synthesized structures for water splitting, we investigate charge distribution and extraction in the Au−ZnO hybrids spectroscopically and electrochemically. Cyclic voltammetry turns out to be a suitable extension to the optical measurements and a powerful technique to directly monitor charge extraction. Thus, we show that the electron extraction is facilitated by the gold demonstrating the potential of our Au−ZnO nanoparticles for photocatalytic applications.

RESULTS AND DISCUSSION

ZnO nanoparticles are formed in a base hydrolyzed colloidal synthesis with oleic acid as the stabilizing agent. The use of oleic acid drives the formation of the pyramidal shape. The energy of each facet is determined by the atomic composition of the facet combined with the attached ligand.[16,24] The ZnO NPs obtained from the synthesis exhibit a wurtzite crystal structure with the *c*-axis along the [002] direction (XRD see Supporting Information), which results in the formation of oxygen-rich (001), zinc-rich ($00\bar{1}$), and mixed facets e.g. (100).[25] Oleic acid forms bonds with zinc atoms,[14] and therefore the facet energy can be qualitatively weighted in the order of E(oxygen rich) > E(mixed surface) > E(zinc rich). Lower energy surfaces are thermodynamically subject to further growth, while higher energy surfaces are minimized. We observe pyramidal shapes only at reaction temperatures >160 °C (Figure 1A). At lower temperatures the synthesis yields slightly elongated or rounded shapes.

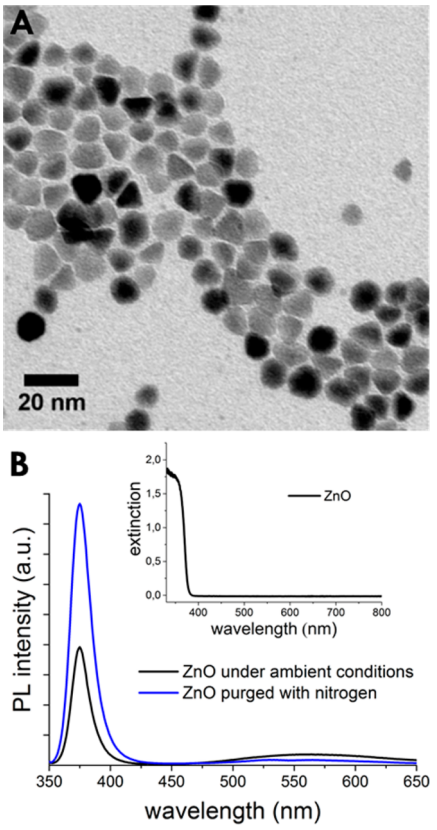

Figure 1. (A) TEM micrograph of pyramidal ZnO NPs. (B) PL spectra of ZnO dispersions recorded under ambient conditions and after being purged with nitrogen.

The size distribution in the ZnO samples strongly depends on the initial size distribution upon injection of the base. The experiments show that an injection temperature of 130 °C yields an initial size distribution of 15% whereas lower and higher temperatures lead to 19% and 20% distributions, respectively (see Supporting Information). An initial broad size distribution always results in further size defocusing during particle growth. Once an initial homogeneous sample is formed, higher temperatures are needed to shift the equilibrium to the pyramidal shape. Therefore, the synthesis is conducted in two steps. After the base is injected at 130 °C to form homogeneous nuclei, the temperature is subsequently increased to 160 °C to form pyramidal nanoparticles.

Oleic acid is not only a significant driving force in shape formation but also influences the precursor formation as well which can have a dramatic effect on the course of the reaction. We investigated ligand to zinc ratios of 1:2, 1:1, and 2:1. Oleic acid is able to substitute the acetate to form zinc oleate, which we confirmed using infrared spectroscopy (IR spectra can be found in the Supporting Information). In the case of 1:2 and 1:1 ratios only mixed precursor species can form; in the case of 2:1 the acetate can be entirely substituted by oleate. A striking difference can be noticed in the case of 2:1 ratio, where particles of ∼100 nm (see Supporting Information) are formed.[26] We observed that only mixed precursor species allow for small particle formation (∼10 nm).

As the semiconducting NP size approaches the size of the Bohr-exciton radius, the band gap significantly enlarges which can be clearly detected in the absorption and emission spectra. In the case of our ZnO nanocrystals, the NPs with a size of 9.5

DOI: 10.1021/acs.jpcc.5b06520
J. Phys. Chem. C 2015, 119, 21704−21710

± 1.6 nm, we observe the absorption edge at 371 nm (Figure 1B, inset). This corresponds to the band gap energy of 3.34 eV, indicating a weak quantum confinement regime.[27]

The good passivation by oleate allows for stable suspensions in organic solvents such as chloroform or toluene and is additionally confirmed by PL spectra (Figure 1B). Whereas the UV band is related to the bandgap relaxation, the so-called green band is attributed to the relaxation from or to bandgap states,[28−33] and its intensity serves as a reliable indicator of the passivation quality.[13] Bandgap states are usually caused by irregularities in the crystal lattice and surface dangling bonds. Depending on the particular relaxation rates, individual maxima can be distinguished,[29] while a broad band is obtained when several emission bands overlap.[32,33] Several defects were identified in ZnO NPs, which contribute to the green luminescence.[31,34,35] Despite ongoing discussion in the literature concerning the individual assignment of the defect states in the PL spectra, the largest contribution to the green luminescence is agreed to be caused by an oxygen vacancy which acts as the shallow acceptor.

PL spectra of ZnO particles were recorded under ambient and nitrogen atmosphere. Changes in emission intensity provide information on recombination pathways. The PL spectra of as-synthesized ZnO NPs (Figure 1B, black curve) show a large band gap emission compared to the green emission, thus revealing a low defect density. This indicates a large well-passivated surface and minimized low passivated facet ((001), oxygen rich). A dramatic change in the PL behavior occurs after purging the ZnO NP solution with nitrogen to remove oxygen from the particle surface (Figure 1B, blue curve). The intensity of the UV emission increases by the factor of 2.2 while the green emission decreases by the factor of 2.1. Since oxygen is known to chemisorb on the surface of n-type ZnO by accepting electrons,[36−38] its presence has an observable effect on the charge recombination dynamics.[39] While oxygen is present, electron density is withdrawn from the NPs. Once an electron in the ZnO NP is excited to the conduction band, it can either relax to the valence band or it can be trapped on the oxygen vacancy site. Further relaxation to the valence band is observed as the green luminescence. By thoroughly purging the sample oxygen is removed, which leads to charge accumulation in the conduction band upon UV illumination. Strong bleaching under these conditions was observed for ZnO particles and electrodes by several groups.[12,39] It is argued to be due either to the Mosse−Burstein[40] or even the Stark effect.[41,42] In that state the recombination over the band gap becomes more likely, and the UV peak intensity increases whereas the green band is subject to an intensity decrease.

Under UV excitation, electrons in ZnO are promoted from the valence band to the conduction band obtaining sufficient potential for the reduction of Au^{3+} to Au^0, causing gold particle formation on the ZnO surface.[20] Interestingly, we observe that gold particles with a size of 3−4 nm are formed exclusively on the tip of the ZnO pyramids under these conditions (Figure 2A). Only particles bound to ZnO, and no free gold particles, were observed in all samples prepared during the whole study. Gold particles formation is easily observed from the absorption spectrum, which reveals a peak at 530 nm, corresponding to the plasmonic band of gold (Figure 2B). In the absence of ZnO or UV excitation no Au particles were formed.

As displayed in the TEM image (Figure 2A), about half of the ZnO structures are decorated by an Au particle. More careful analysis of the TEM image reveals that the ZnO

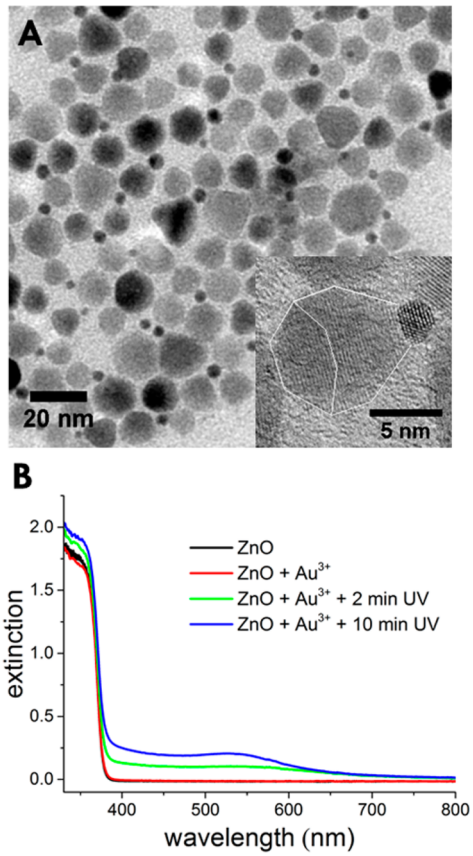

Figure 2. (A) TEM micrographs of Au−ZnO hybrid structures. The inset shows a high-resolution image of a single Au−ZnO NP. (B) Extinction spectra of a ZnO NP dispersions before and upon addition of Au^{3+} salt without and with UV illumination.

structures with a gold NP attached at the tip exhibit a more pronounced pyramidal structure than the bare ones (see inset in Figure 2B). This indicates that the presence of the well-defined tip is crucial for the gold formation. Increased gold precursor concentration yields fewer larger gold particles rather than more smaller particles on the ZnO tips (see Supporting Information), indicating that particle morphology is decisive for the Au NP formation.

Selective growth of metal particles on semiconducting structures is determined by the interplay between crystal plane composition, surface morphology, and electronic structure.[43] The composition of ZnO crystal planes decides on their polarity; crystal planes consisting of monolayers of either zinc $(00\bar{1})$ or oxygen (001) are polar. All other planes are mixed and nonpolar. It was shown that the polar facets of ZnO are far more photocatalytically active than the nonpolar surfaces.[44] This is attributed to the higher concentration of oxygen vacancies on polar surfaces which would increase the probability of charge separation[45] and charge transfer.[44,46]

In the case of the pyramidal ZnO nanocrystals, the morphology of the surface is determined by the oleic acid attached to it, which acts as a stabilizing agent. It binds as oleate to Zn^{2+} at the surface,[14] yielding well-stabilized zinc-rich $(00\bar{1})$ and mixed facets. However, the oxygen-rich tip (001) is not likely to build any strong chemical bonds with the oleate. Growth is along the *c*-axis (XRD see Supporting Information) in the direction of [002]. This would indicate that the pyramidal base is formed by the $(00\bar{1})$ facet, which consists of a

DOI: 10.1021/acs.jpcc.5b06520
J. Phys. Chem. C 2015, 119, 21704−21710

monolayer of zinc atoms stabilized by oleic acid. The (001) facet, on the other hand, is oxygen rich and is reduced in area to form the pyramid tip. Enhanced charge separation and transfer efficiency at the tip could favor the reduction of Au ions leading to the localized formation of Au particles.

First-principles-based calculation performed by Yao et al.[20] argues that the lowest unoccupied state in ZnO pyramids is provided by mainly Zn-sp state. On the basis of the calculation, they conclude that the light-induced gold formation on the tip of big (60−70 nm) pyramids is solely driven by the availability of unoccupied states at the vertex of the pyramid. In contrast to our synthesis, the ZnO particles were prepared using a hydrothermal method without ligand addition. As discussed for ZnO preparation, oleic acid plays a crucial role not only in formation but also in stabilizing the surface of the nano-pyramids, which we are considering here.

In order to confirm our hypothesis about the mechanism of gold particles formation, DFT calculations were performed. An Au^0 atom was placed in close proximity to different facets of a small ZnO cluster (48 Zn/48 O) as shown in Figure 3. While

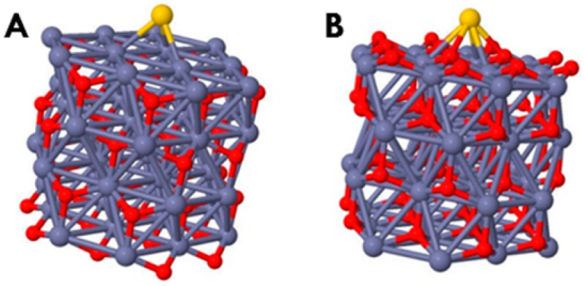

Figure 3. Simulated ZnO (Zn gray, O red) cluster with a gold atom bound to the (A) zinc-rich (00$\bar{1}$) and (B) oxygen-rich (001) facet.

the ZnO cluster was kept fixed in its geometry with the experimental lattice constant, the Au atom was allowed to relax in time. The results of these simulations describe the stability of the simplified heterostructure where Au has already been reduced. The energy differences between the sum of the two separated systems and the combined system after relaxation give a hint for the stability of Au on different facets. Also, the stability of oleic acid and oleate was tested. The neutral oleic acid binds only weakly to all facets. The energy difference of oleate attached to the zinc-rich surface is the highest, which corresponds to the chemical bond of negatively charged oleate and positively charged zinc. These calculations support the hypothesis of the ligand-driven ZnO pyramid formation.

The comparison of the energetics for the case of Au−ZnO versus oleate−ZnO shows that the energy gain for the configuration where oleate is attached to the zinc-rich facet is larger than for the situation where gold is attached to the same facet, making the Au−ZnO formation unlikely, whereas in the case of oleate at the oxygen-rich surface the energy gain is lower than for gold attachment at the same surface. It is worth noting that the adsorption energy gain for Au bound to zinc-rich versus Au bound to oxygen-rich facets is very comparable if the oleic acid attachment is neglected. That means that according to the presented theoretical considerations, Au is likely to bind to either of the sites. These results imply that the surfactants make one of the polar facets (in this case oxygen-rich (001)) more favorable for the Au formation.

We then studied the influence of gold particles on charge distribution in the Au−ZnO hybrids. To do this, we performed steady state PL on the ZnO NPs in the presences of gold salt. Very interestingly, the comparison of the PL spectra prior to the $AuCl_3$ addition and after reveals striking differences (Figure 4A). In contrast to the spectra of ZnO in the absence of gold

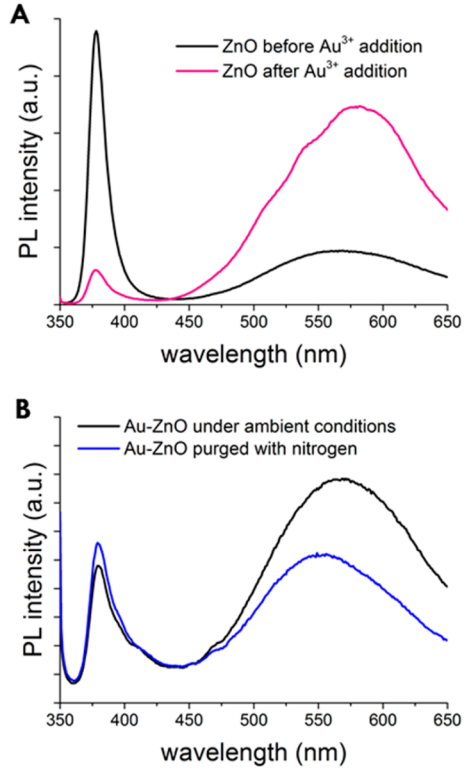

Figure 4. (A) PL spectra of ZnO dispersions before and upon Au^{3+} salt addition. (B) PL spectra of presynthesized Au−ZnO NP dispersions recorded under ambient conditions and after purging with nitrogen. An excitation wavelength of 340 nm was used in all PL measurements.

salt, the UV emission is suppressed and the green emission increases drastically when $AuCl_3$ is added. For a comparison, we also measured the PL of ready synthesized and washed Au−ZnO samples where the gold salt excess was removed (Figure 4B). These spectra show similar behavior although the ratio between the UV and the green luminescence is lower than in the case of *in situ* synthesis. Suppression of the UV band in Figure 4A supports the hypothesis that photoexcited electrons in ZnO are consumed by the gold reduction, since their chemical potential is sufficient to drive the reaction (Figure 5). In the case of presynthesized hybrid particles the UV band suppression in Figure 4B is not as significant and is more likely due to electron transfer to the gold, which has a Fermi energy (−5.3 eV) higher than the conduction band edge of ZnO NPs (−4.41 eV, determined from cyclovoltammograms). This behavior is in agreement with published studies.[12,39]

The PL data reveal that charge transfer between ZnO and gold influences the relative dynamics of recombination in the ZnO particles. This causes the suppression of the UV band emission and increase in green emission. From the PL spectra, the energy of defect states resulting in green emission is found to be between −5.65 and −5.25 eV. This corresponds to a value equal to or below the Fermi energy of gold. The relative

DOI: 10.1021/acs.jpcc.5b06520
J. Phys. Chem. C 2015, 119, 21704−21710

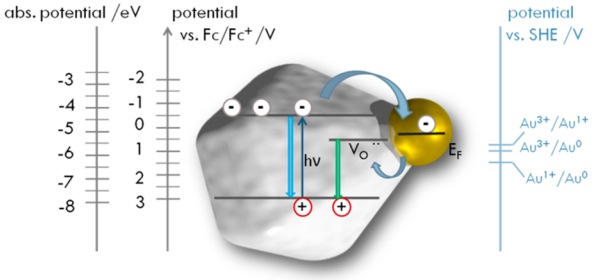

Figure 5. Band diagram of Au−ZnO hybrids including electronic and electrochemical potential scales.

increase in green emission would then be governed by favorable charge transfer between the gold and the defect states (Figure 5). This process, in combination with a bleaching of the ZnO particle, would lead to the observed changes in PL emission between ZnO in the presence and absence of gold. It should be noted that green emission intensity can additionally be enhanced by plasmonic coupling as the plasmonic band of the gold particle (530 nm) overlaps with the defect emission band.

The PL results strongly support the concept of electron transfer from the conduction band of ZnO to the gold particle. In order to confirm that the Au particles act as an electron extraction site, cyclic voltammetry was performed. This method allows for determination of energy levels upon charge injection (corresponds to the cathodic peak) and charge extraction (corresponds to the anodic peak). Ideally, every energy level yields a pair of anodic and cathodic peaks. The voltammogramms of the ZnO samples with and without illumination are shown in Figure 6A. The data reveal that the cathodic peak at −0.9 V, corresponding to the LUMO level, is pronounced whereas the anodic peak is suppressed for both the dark and light cases. Instead, the higher energy anodic peak at −1.2 V in dark and at −1.1 V under illumination is visible. On the basis of this, we can conclude that the charge injected into the LUMO level at −0.9 V is lost to the green emission pathway and therefore cannot be extracted.

We compare these data to voltammograms taken from Au−ZnO in Figure 6B. In the dark, electron injection is observed at −0.8 V, but the peak associated with extraction is not detected for the LUMO as well as for higher energy levels. This is attributed to efficient charge transfer from ZnO to the gold and further loss over the defect emission pathway. In contrast, when the hybrid structures are illuminated, the LUMO peak associated with electron extraction at −0.3 V is observed, demonstrating facilitated electron extraction. We note that in cyclic voltammetry differences in electronic structure of the samples is apparent from the differences in onset potent, as described. Differences in the current, however, are related to differences in the rate of electron transfer reactions at the electrode interface. This is relatively trivial in the case of ZnO compared to Au−ZnO samples and can be related to slight variations in processing or film thickness.

Using PL spectroscopy, we were able to demonstrate charge redistribution in Au−ZnO nanohybrids. Cyclic voltammetry was then used to confirm enhanced electron extraction efficiency from the hybrid systems. This work shows that combining optical and electrochemical methods is a powerful strategy to study the correlation between charge distribution

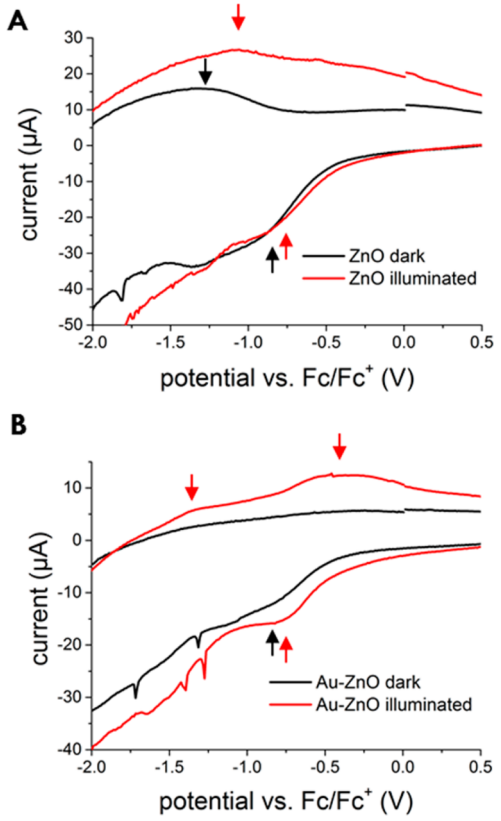

Figure 6. Cyclic voltammograms of (A) ZnO NPs and (B) Au−ZnO hybrids recorded in dark and under illumination. Arrows are indicating the peaks, which are described in the text.

and electrochemical activity in photocatalysts, e.g., for water splitting applications.

CONCLUSIONS

We demonstrated a two-step synthesis of very small Au−ZnO hybrids (10 nm). A directed photochemical deposition of gold NPs led to controlled Au particle formation exclusively on the tip of ZnO nanopyramids. The Au particle forms an electron extraction site facilitating charge transfer at the ZnO surface. We monitored simultaneously changes in band gap and defect luminescence intensities, which revealed excited electron transfer from ZnO to Au leading to suppression of band gap emission. We conclude that the electron extraction barrier in ZnO, observed with cyclic voltammetry, is overcome by channeling the electrons through gold NPs on the ZnO tip. That means that creating well-defined hybrid Au−ZnO nanostructures alters the catalytic behavior of pristine ZnO allowing for facilitated electron extraction, which is beneficial for photocatalytic activity.

EXPERIMENTAL SECTION

Chemicals. Zinc acetate dihydrate (Merck, p.a.), 2-phenylethanol (Sigma-Aldrich, ≥99.9%), oleic acid (Sigma-Aldrich, 90%), methanol (Sigma-Aldrich, ≥99.9%), chloroform (Sigma-Aldrich, ≥99%), gold(III) chloride (Sigma-Aldrich, ≥99.99%), tetra-*n*-butylammonium hexafluorophosphate (Fluka, ≥99.0%), acetonitrile (Merck, water free), ferrocene (Sigma-Aldrich, 98%), and silver nitrate (VWR, p.a.).

ZnO Nanopyramid Synthesis. The amount of 0.27 g (1.2 mmol) of zinc acetate dihydrate was dissolved in 10 mL of 2-

DOI: 10.1021/acs.jpcc.5b06520
J. Phys. Chem. C 2015, 119, 21704−21710

phenylethanol. After heating the solution up to 60 °C, 0.42 mL (1.3 mmol) of oleic acid was added. As soon as the temperature of the mixture reached 130 °C, 6.5 mL of a 0.4 M potassium hydroxide solution were added. The obtained mixture was stirred for 2 h at 160 °C. The ZnO precipitate was separated from the solution by centrifugation and subsequently cleaned twice with a methanol/chloroform mixture. Finally, cleaned particles were stored in chloroform.

Au−ZnO Hybrid Synthesis. The suspension of ZnO NPs (0.20 mg/mL) and gold(III) chloride (0.01 mg/mL) was prepared in a quartz cuvette with a total volume of 3 mL of chloroform. After UV irradiation at 254 nm for 2−10 min, the product was separated from the solvent by centrifugation and resuspended in chloroform.

TEM Characterization. For TEM characterization a LEO Omega 912 transmission electron microscope with an acceleration voltage of 120 kV by Zeiss was employed. High-resolution micrographs were obtained with JEOL JEM-2200FS microscope with c_s correctors at an acceleration voltage of 200 kV.

X-ray Diffractometry. X-ray diffractogramms were collected using Philips X'Pert diffractrometer with a copper cathode and nickel filter (λ = 154.178 nm).

Infrared Spectroscopy. IR measurements were performed on a FT-IR Vairan 660 spectrometer with an ATR unit.

Absorption Spectroscopy. A Lambda 25 UV−vis spectrometer by PerkinElmer was used to collect absorption spectra of ZnO and Au−ZnO NPs suspended in chloroform.

Photoluminescence Spectroscopy. All spectra were recorded using the Fluoromax-4 spectrofluorometer by Horiba Scientific. All samples were measured in suspension while excited at 340 nm. For measurements shown in Figure 4A, a suspension of ZnO NPs (0.20 mg/mL) as well as a suspension of ZnO NPs (0.20 mg/mL) and gold(III) chloride (0.01 mg/mL) was used. To obtain spectra displayed in Figure 4B, Au−ZnO samples were prepared following the procedure for Au−ZnO synthesis described above. The purified product was resuspended in the same amount of chloroform, yielding a comparable concentration to the initial concentration of ZnO NPs. In this case we did not account for material losses during purification.

Cyclic Voltammetry. The measurements were performed under inert atmosphere. A tetra-*n*-butylammonium hexafluorophosphate solution (0.1 M) in acetonitrile was used as electrolyte with ferrocene as an internal standard. Platinum mesh electrode and a silver/silver nitrite electrode served as counter and pseudo reference electrodes, respectively. The ZnO and Au-ZnO samples were drop-casted on the indium tin oxide ($R_{sq} \leq 10\ \Omega/\square$) working electrode prior to measurement. Autolab PGSTAT302N by Metrohm was used to collect the voltammograms.

Theoretical Methods. The adsorption energy of an Au^0 atom on a ZnO cluster was calculated in the frame of the density functional theory (DFT) by subtracting the sum of the separated systems form the combined one. The geometry of the atoms in the ZnO cluster was kept fixed with the experimental lattice constant while the Au atom was free to relax. For the calculations the ORCA software[47] was used with the LDA exchange functional, the correlation functional VWN-5[48] and the Ahlrichs TZV basis set[49] served as the framework for the calculations. For the gold an LANLTZ basis set was used.[50] In order to save computation time, oleic acid and the oleate were replaced for a shorter version of the molecule with three carbon atoms (propanoic acid). This does not change the qualitative results.

■ ASSOCIATED CONTENT

Supporting Information

The Supporting Information is available free of charge on the ACS Publications website at DOI: 10.1021/acs.jpcc.5b06520.

Additional TEM micrographs as described in the article, IR spectroscopical data, X-ray diffractogram of ZnO nanocrystals (PDF)

■ AUTHOR INFORMATION

Corresponding Author

*E-mail a.chanaewa@vu.nl (A.C.).

Present Address

A.C.: Physics of Energy, VU University Amsterdam, 1081HV Amsterdam, Netherlands.

Funding

This work was performed as a part of Organic Photovoltaics Project funded by Fraunhofer ISE Freiburg, Germany.

Notes

The authors declare no competing financial interest.

■ ACKNOWLEDGMENTS

Dr. Ralf Thomann and Daniela Weinert are gratefully acknowledged for TEM characterization. A.C. thanks Rut von Waldenfels for support with cyclic voltammetry meas-urements. A.C., J.S., and E.v.H. thank Stefan Glunz and the Fraunhofer ISE in Freiburg (Germany) for support.

■ REFERENCES

(1) Bard, A. J.; Fox, M. A. Artificial Photosynthesis: Solar Splitting of Water to Hydrogen and Oxygen. *Acc. Chem. Res.* **1995**, *28*, 141−145.

(2) Chen, X.; Liu, L.; Yu, P. Y.; Mao, S. S. Increasing Solar Absorption for Photocatalysis with Black Hydrogenated Titanium Dioxide Nanocrystals. *Science* **2011**, *331*, 746−750.

(3) Zou, Z.; Ye, J.; Sayama, K.; Arakawa, H. Direct Splitting of Water under Visible Light Irradiation with an Oxide Semiconductor Photocatalyst. *Nature* **2001**, *414*, 625−627.

(4) Bolton, J. R.; Strickler, S. J.; Connolly, J. S. Limiting and Realizable Efficiencies of Solar Photolysis of Water. *Nature* **1985**, *316*, 495−500.

(5) Hu, Z.; Oskam, G.; Searson, P. C. Influence of Solvent on the Growth of ZnO Nanoparticles. *J. Colloid Interface Sci.* **2003**, *263*, 454−460.

(6) Kahn, M. L.; Monge, M.; Collière, V.; Senocq, F.; Maisonnat, A.; Chaudret, B. Size- and Shape-Control of Crystalline Zinc Oxide Nanoparticles: A New Organometallic Synthetic Method. *Adv. Funct. Mater.* **2005**, *15*, 458−468.

(7) Wong, E. M.; Hoertz, P. G.; Liang, C. J.; Shi, B.-M.; Meyer, G. J.; Searson, P. C. Influence of Organic Capping Ligands on the Growth Kinetics of ZnO Nanoparticles. *Langmuir* **2001**, *17*, 8362−8367.

(8) Coppa, B. J.; Fulton, C. C.; Kiesel, S. M.; Davis, R. F.; Pandarinath, C.; Burnette, J. E.; Nemanich, R. J.; Smith, D. J. Structural, Microstructural, and Electrical Properties of Gold Films and Schottky Contacts on Remote Plasma-Cleaned, n-type ZnO{0001} Surfaces. *J. Appl. Phys.* **2005**, *97*, 103517.

(9) Hotchandani, S.; Kamat, P. V. J. Photoelectrochemistry of Semiconductor ZnO Particulate Films. *J. Electrochem. Soc.* **1992**, *139*, 1630−1634.

(10) Subramanian, V.; Wolf, E. E.; Kamat, P. V. Catalysis with TiO_2/Gold Nanocomposites. Effect of Metal Particle Size on the Fermi Level Equilibration. *J. Am. Chem. Soc.* **2004**, *126*, 4943−4950.

DOI: 10.1021/acs.jpcc.5b06520
J. Phys. Chem. C 2015, 119, 21704−21710

(11) Jakob, M.; Levanon, H.; Kamat, P. V. Charge Distribution between UV-Irradiated TiO_2 and Gold Nanoparticles: Determination of Shift in the Fermi Level. *Nano Lett.* **2003**, *3*, 353−358.
(12) Wood, A.; Giersig, M.; Mulvaney, P. Fermi Level Equilibration in Quantum Dot-Metal Nanojunctions. *J. Phys. Chem. B* **2001**, *105*, 8810−8815.
(13) Chen, Y.; Kim, M.; Lian, G.; Johnson, M. B.; Peng, X. Side Reactions in Controlling the Quality, Yield, and Stability of High Quality Colloidal Nanocrystals. *J. Am. Chem. Soc.* **2005**, *127*, 13331−13337.
(14) Choi, S.-H.; Kim, E.-G.; Park, J.; An, K.; Lee, N.; Kim, S. C.; Hyeon, T. Large-Scale Synthesis of Hexagonal Pyramid-Shaped ZnO Nanocrystals from Thermolysis of Zn-Oleate Complex. *J. Phys. Chem. B* **2005**, *109*, 14792−14794.
(15) Meulenkamp, E. A. Synthesis and Growth of ZnO Nanoparticles. *J. Phys. Chem. B* **1998**, *102*, 5566−5572.
(16) Yin, Y.; Alivisatos, A. P. Colloidal Nanocrystal Synthesis and the Organic-Inorganic Interface. *Nature* **2005**, *437*, 664−670.
(17) Joo, J.; Kwon, S.; Yu, J.; Hyeon, T. Synthesis of ZnO Nanocrystals with Cone, Hexagonal Cone, and Rod Shapes via Non-Hydrolytic Ester Elimination Sol−Gel Reactions. *Adv. Mater.* **2005**, *17*, 1873−1877.
(18) Herring, N. P.; AbouZeid, K.; Mohamed, M. B.; Pinsk, J.; El-Shall, M. S. Formation Mechanisms of Gold-Zinc Oxide Hexagonal Nanopyramids by Heterogeneous Nucleation using Microwave Synthesis. *Langmuir* **2011**, *27*, 15146−15154.
(19) Li, P.; Wei, Z.; Wu, T.; Peng, Q.; Li, Y. Au-ZnO Hybrid Nanopyramids and Their Photocatalytic Properties. *J. Am. Chem. Soc.* **2011**, *133*, 5660−5663.
(20) Yao, K. X.; Liu, X.; Zhao, L.; Zeng, H. C.; Han, Y. Site-Specific Growth of Au Particles on ZnO Nanopyramids under Ultraviolet Illumination. *Nanoscale* **2011**, *3*, 4195−4200.
(21) Zhou, X.; Xie, Z.-X.; Jiang, Z.-Y.; Kuang, Q.; Zhang, S.-H.; Xu, T.; Huang, R.-B.; Zheng, L.-S. Formation of ZnO Hexagonal Micro-Pyramids: a Successful Control of the Exposed Polar Surfaces with the Assistance of an Ionic Liquid. *Chem. Commun.* **2005**, 5572−5574.
(22) Li, P.; Wang, D.; Wei, Z.; Peng, Q.; Li, Y. Systematic Synthesis of ZnO Nanostructures. *Chem. - Eur. J.* **2013**, *19*, 3735−3740.
(23) Yue, M.; Yang, M.; Zhang, D.; Xiang, D.; Hou, Y.; Han, J. Hybrid Au/ZnO Hexagonal Pyramid Nanostructures: Preferred Growth on the Apexes of the Basal Plane than on the Tip. *J. Phys. Chem. C* **2015**, *119*, 4199−4207.
(24) Puzder, A.; Williamson, A. J.; Zaitseva, N.; Galli, G.; Manna, L.; Alivisatos, A. P. The Effect of Organic Ligand Binding on the Growth of CdSe Nanoparticles Probed by *Ab Initio* Calculations. *Nano Lett.* **2004**, *4*, 2361−2365.
(25) Laudise, R. A.; Ballman, A. A. Hydrothermal Synthesis of Zinc Oxide and Zinc Sulfide. *J. Phys. Chem.* **1960**, *64*, 688−691.
(26) Chiu, W.; Khiew, P.; Isa, D.; Cloke, M.; Radiman, S.; Abd-Shukor, R.; Abdullah, M.; Huang, N. Synthesis of Two-Dimensional ZnO Nanopellets by Pyrolysis of Zinc Oleate. *Chem. Eng. J.* **2008**, *142*, 337−343.
(27) Viswanatha, R.; Sapra, S.; Satpati, B.; Satyam, P. V.; Dev, B. N.; Sarma, D. D. Understanding the Quantum Size Effects in ZnO Nanocrystals. *J. Mater. Chem.* **2004**, *14*, 661−668.
(28) Gong, Y.; Andelman, T.; Neumark, G.; O'Brien, S.; Kuskovsky, I. Origin of Defect-Related Green Emission from ZnO Nanoparticles: Effect of Surface Modification. *Nanoscale Res. Lett.* **2007**, *2*, 297−302.
(29) Irimpan, L.; Nampoori, V. P. N.; Radhakrishnan, P.; Deepthy, A.; Krishnan, B. Size Dependent Fluorescence Spectroscopy of Nanocolloids of ZnO. *J. Appl. Phys.* **2007**, *102*, 063524.
(30) Leiter, F.; Alves, H.; Hofstaetter, A.; Hofmann, D.; Meyer, B. The Oxygen Vacancy as the Origin of a Green Emission in Undoped ZnO. *Phys. Status Solidi B* **2001**, *226*, R4−R5.
(31) Vanheusden, K.; Warren, W. L.; Seager, C. H.; Tallant, D. R.; Voigt, J. A.; Gnade, B. E. Mechanisms behind Green Photoluminescence in ZnO Phosphor Powders. *J. Appl. Phys.* **1996**, *79*, 7983−7990.
(32) Xu, P.; Sun, Y.; Shi, C.; Xu, F.; Pan, H. The Electronic Structure and Spectral Properties of ZnO and its Defects. *Nucl. Instrum. Methods Phys. Res., Sect. B* **2003**, *199*, 286−290.
(33) Zheng, Y.; Chen, C.; Zhan, Y.; Lin, X.; Zheng, Q.; Wei, K.; Zhu, J.; Zhu, Y. Luminescence and Photocatalytic Activity of ZnO Nanocrystals: Correlation between Structure and Property. *Inorg. Chem.* **2007**, *46*, 6675−6682.
(34) Lin, B.; Fu, Z.; Jia, Y. Green Luminescent Center in Undoped Zinc Oxide Films Deposited on Silicon Substrates. *Appl. Phys. Lett.* **2001**, *79*, 943−945.
(35) van Dijken, A.; Meulenkamp, E. A.; Vanmaekelbergh, D.; Meijerink, A. The Kinetics of the Radiative and Nonradiative Processes in Nanocrystalline ZnO Particles upon Photoexcitation. *J. Phys. Chem. B* **2000**, *104*, 1715−1723.
(36) Chanaewa, A.; Juarez, B. H.; Weller, H.; Klinke, C. Oxygen and Light Sensitive Field-Effect Transistors Based on ZnO Nanoparticles Attached to Individual Double-Walled Carbon Nanotubes. *Nanoscale* **2012**, *4*, 251−256.
(37) Jin, Y.; Wang, J.; Sun, B.; Blakesley, J. C.; Greenham, N. C. Solution-Processed Ultraviolet Photodetectors Based on Colloidal ZnO Nanoparticles. *Nano Lett.* **2008**, *8*, 1649−1653.
(38) Kind, H.; Yan, H.; Messer, B.; Law, M.; Yang, P. Nanowire Ultraviolet Photodetectors and Optical Switches. *Adv. Mater.* **2002**, *14*, 158−160.
(39) Subramanian, V.; Wolf, E. E.; Kamat, P. V. Green Emission to Probe Photoinduced Charging Events in ZnO-Au Nanoparticles. Charge Distribution and Fermi-Level Equilibration. *J. Phys. Chem. B* **2003**, *107*, 7479−7485.
(40) Burstein, E. Anomalous Optical Absorption Limit in InSb. *Phys. Rev.* **1954**, *93*, 632−633.
(41) Colvin, V. L.; Cunningham, K. L.; Alivisatos, A. P. Electric Field Modulation Studies of Optical Absorption in CdSe Nanocrystals: Dipolar Character of the Excited State. *J. Chem. Phys.* **1994**, *101*, 7122−7138.
(42) Hilinski, E. F.; Lucas, P. A.; Wang, Y. A Picosecond Bleaching Study of Quantum-Confined Cadmium Sulfide Microcrystallites in a Polymer Film. *J. Chem. Phys.* **1988**, *89*, 3435−3441.
(43) Costi, R.; Saunders, A.; Banin, U. *Angew. Chem., Int. Ed.* **2010**, *49*, 4878−4897.
(44) Mclaren, A.; Valdes-Solis, T.; Li, G.; Tsang, S. C. Shape and Size Effects of ZnO Nanocrystals on Photocatalytic Activity. *J. Am. Chem. Soc.* **2009**, *131*, 12540−12541.
(45) Li, G. R.; Hu, T.; Pan, G. L.; Yan, T. Y.; Gao, X. P.; Zhu, H. Y. Morphology-Function Relationship of ZnO: Polar Planes, Oxygen Vacancies, and Activity. *J. Phys. Chem. C* **2008**, *112*, 11859−11864.
(46) Pacholski, C.; Kornowski, A.; Weller, H. Site-Specific Photodeposition of Silver on ZnO Nanorods. *Angew. Chem.* **2004**, *116*, 4878−4881.
(47) Neese, F. WIREs Site-Specific Photodeposition of Silver on ZnO Nanorods. *Comput. Mol. Sci.* **2012**, *2*, 73−78.
(48) Vosko, S. H.; Wilk, L.; Nusair, M. Accurate Spin-Dependent Electron Liquid Correlation Energies for Local Spin Density Calculations: a Critical Analysis. *Can. J. Phys.* **1980**, *58*, 1200−1211.
(49) Schäfer, A.; Horn, H.; Ahlrichs, R. Fully Optimized Contracted Gaussian Basis Sets for Atoms Li to Kr. *J. Chem. Phys.* **1992**, *97*, 2571−2577.
(50) Roy, L. E.; Hay, P. J.; Martin, R. L. Revised Basis Sets for the LANL Effective Core Potentials. *J. Chem. Theory Comput.* **2008**, *4*, 1029−1031.

DOI: 10.1021/acs.jpcc.5b06520
J. Phys. Chem. C 2015, 119, 21704−21710